



# Derivation and Clinical Validation of a Redox-Driven Prognostic Signature for Colorectal Cancer

Qin Dang<sup>1,2†</sup>, Zaoqu Liu<sup>3,4†</sup>, Shengyun Hu<sup>1</sup>, Zhuang Chen<sup>1</sup>, Lingfang Meng<sup>5</sup>, Junhong Hu<sup>1</sup>, Guixian Wang<sup>1</sup>, Weitang Yuan<sup>1</sup>, Xinwei Han<sup>3,4</sup>, Lifeng Li<sup>6\*</sup> and Zhenqiang Sun<sup>1,2\*</sup>

## OPEN ACCESS

### Edited by:

Nicola Schiavone,  
University of Florence, Italy

### Reviewed by:

János László Hunyadi,  
National Institute of Oncology (NIO),  
Hungary

Jinhui Liu,

Nanjing Medical University, China

Song Li,

Qilu Second Hospital of Shandong

University, China

Jingjing Song,

Second Affiliated Hospital and Yuying

Children's Hospital of Wenzhou

Medical University, China

### \*Correspondence:

Zhenqiang Sun

fccsunzq@zzu.edu.cn

Lifeng Li

lilifeng0317@163.com

<sup>†</sup>These authors have contributed  
equally to this work and share  
first authorship

### Specialty section:

This article was submitted to

Gastrointestinal Cancers:

Colorectal Cancer,

a section of the journal

Frontiers in Oncology

**Received:** 19 July 2021

**Accepted:** 05 October 2021

**Published:** 27 October 2021

### Citation:

Dang Q, Liu Z, Hu S, Chen Z, Meng L,

Hu J, Wang G, Yuan W, Han X, Li L

and Sun Z (2021) Derivation and Clinical

Validation of a Redox-Driven Prognostic

Signature for Colorectal Cancer.

Front. Oncol. 11:743703.

doi: 10.3389/fonc.2021.743703

<sup>1</sup> Department of Colorectal Surgery, The First Affiliated Hospital of Zhengzhou University, Zhengzhou, China, <sup>2</sup> Academy of Medical Sciences, Zhengzhou University, Zhengzhou, China, <sup>3</sup> Department of Interventional Radiology, The First Affiliated Hospital of Zhengzhou University, Zhengzhou, China, <sup>4</sup> Interventional Institute of Zhengzhou University, Zhengzhou, China, <sup>5</sup> Department of Ultrasound, Zhengzhou Sixth People's Hospital, Henan Infectious Disease Hospital, Zhengzhou, China, <sup>6</sup> Internet Medical and System Applications of National Engineering Laboratory, Zhengzhou, China

Colorectal cancer (CRC), a seriously threat that endangers public health, has a striking tendency to relapse and metastasize. Redox-related signaling pathways have recently been extensively studied in cancers. However, the study and potential role of redox in CRC remain unelucidated. We developed and validated a risk model for prognosis and recurrence prediction in CRC patients *via* identifying gene signatures driven by redox-related signaling pathways. The redox-driven prognostic signature (RDPS) was demonstrated to be an independent risk factor for patient survival (including OS and RFS) in four public cohorts and one clinical in-house cohort. Additionally, there was an intimate association between the risk score and tumor immune infiltration, with higher risk score accompanied with less immune cell infiltration. In this study, we used redox-related factors as an entry point, which may provide a broader perspective for prognosis prediction in CRC and have the potential to provide more promising evidence for immunotherapy.

**Keywords:** colorectal cancer, redox, gene signature, prognosis, immune infiltration

## INTRODUCTION

The incidence and mortality of colorectal cancer (CRC) are increasing worldwide (1, 2). Studies have predicted that within the next decade, it is estimated that 1 in 10 colon cancers and 1 in 4 rectal cancers are diagnosed in adults younger than 50 years (3). Limited by the choice of appropriate surgery timing and the operative range, and drug resistance to chemotherapy, malignant events such as adverse prognosis and metastasis in CRC patients are still intractable clinical problems (4, 5). However, when treatment involving surgery, chemoradiotherapy, and targeted therapy fails, no alternative therapy modality is yet available. Recently, immunotherapy has begun to take off in the treatment of tumors (6–9). Nevertheless, our clinical practice shows that not all patients respond well to immunotherapy. Therefore, there is an urgent need to develop a novel strategy to identify patients who are suitable for immunotherapy to facilitate prognostic management and personalized treatment of CRC.

The redox status of cells directly regulates biomacromolecular functions and mediates cell signal transduction as well as many physiological and pathological processes such as senility, metabolic diseases, and tumors (10–12). An altered redox status accompanied with an elevated generation of reactive oxygen/nitrogen species has been implicated in various diseases including CRC (13–15). Numerous studies have reported that CRC is associated with multiple factors such as obesity, dietary patterns, and physical inactivity, resulting in exacerbated oxidative stress with genomic instability (16–18). Recently, innovative therapeutic strategies to target the specific metabolic phenotype of cancer stem cells have been pointed out (19). It determines the self-renewal of CRC stem cells by promoting lactate dehydrogenase A (LDHA) phosphorylation, which in turn treats CRC patients with recurrence and poor outcomes. Additionally, Shashni et al. proposed that reactive oxygen species are the basis of angiogenesis and tumor growth, and the use of antioxidants may be an effective method to impair tumors (20). Collectively, redox-related targets may modulate the pathophysiological behavior of malignant colorectal tumors, suggesting potential clinical utility.

Accumulating studies revealed that the antioxidant defense network alleviates oxidative stress, regulates inflammatory responses, and improves immunity by ensuring redox balance and adaptive homeostasis (21–23). The rapid development of sequencing technology offers more possibilities for identifying more valuable tumor markers (24, 25). We previously studied the relationship between distinct immune classification and immunotherapy, and an immune miRNA signature for assessing prognosis and immune landscape of patients with CRC (26, 27). We hope to explore the relationship with the prognosis and recurrence of CRC by following the novel insight of redox.

In this study, we systematically investigated the dysregulation of redox-related pathways in CRC, and based on the redox-related genes, we constructed a redox-related signature in the TCGA-CRC cohort. Subsequent validation was performed in three independent cohorts from the GEO database. We further verified the stability and accuracy of the RDPS model in a clinical in-house cohort. In addition, the molecular characteristics, inflammation landscape, and immune checkpoint profiles of this signature were investigated. Taken together, RDPS might be a reliable and promising biomarker in CRC.

## MATERIALS AND METHODS

### Public Data Collection and Processing

We retrospectively collected four CRC cohorts from The Cancer Genome Atlas (TCGA, <https://portal.gdc.cancer.gov>) and Gene Expression Omnibus (GEO, <http://www.ncbi.nlm.nih.gov/geo>) databases, including TCGA-CRC, GSE17536, GSE29621, and GSE39582. The RNA-seq raw read count from the TCGA database was converted to transcripts per kilobase million (TPM) and further log<sub>2</sub> transformed. Data from GEO belong to the Affymetrix<sup>®</sup> GPL570 platform ([HG-U133 Plus 2]

Affymetrix<sup>®</sup> Human Genome U133 Plus 2.0 Array). The raw data from Affymetrix<sup>®</sup> were processed using the robust multi-array averaging (RMA) algorithm implemented in the affy R package. RMA was used to perform background adjustment, quantile normalization, and final summarization of oligonucleotides per transcript using the median polish algorithm. In three cohorts, we only retained CRC patients that met the following criteria: (1) primary tumor tissues samples; (2) no preoperative chemotherapy or radiotherapy received; (3) RNA expression data available; and (4) survival information is available and survival time is not zero. A total of 595 patients from TCGA-CRC were used as the training set, and GSE17536 (n = 194), GSE29621 (n = 65), and GSE39582 (n = 595) from the GEO database were used as the validation sets. The corresponding clinical information of the four cohorts was also downloaded, and the demographic data are summarized in **Supplementary Table S1**.

### Signature Generation

First, based on univariate Cox regression, we identified stable prognosis-associated genes. Second, using the expression of these prognosis-associated genes in TCGA-CRC, we fitted a LASSO Cox regression model for assessing the prognosis of patients. Using the 10-fold cross validations, the optimal lambda was obtained when the partial likelihood deviance reached the minimum value. We choose lambda *via* 1-SE (standard error) criteria. The optimal lambda is the largest value for which the partial likelihood deviance is within one SE of the smallest value of partial likelihood deviance. Third, based on the selected lambda, the prognosis-associated genes with nonzero coefficients were selected to construct the prediction signature. The RDPS score was calculated using the coefficient weighted by the Cox model as follows:

$$RDPS\ score = \sum_{i=1}^n Exp_i \times Coef_i$$

where *n* is the number of key prognosis-associated genes, *Exp<sub>i</sub>* is the expression of prognosis-associated gene *i*, and *Coef<sub>i</sub>* is the LASSO coefficient of prognosis-associated gene *i*.

### Delineate the Mutation Landscape

In order to compare the molecular differences of genomic mutations between the high-risk and low-risk groups, we processed the mutated MAF file encompassing somatic alterations *via* the VarScan pipeline. The maftools package was further utilized to visualize the mutation waterfall plots. Genes with mutation frequency greater than 10% were included for further analysis.

### Functional Enrichment and Immune Infiltration Analysis

To explore the potential functional differences of pathways with high and low risk scores, the gene set enrichment analysis (GSEA) algorithm was performed to identify dramatically enriched terms related to the Kyoto Encyclopedia of Genes and Genomes (KEGG) pathway and the biological process of gene

ontology (GO). Permutations were set to 1,000 to obtain a normalized enrichment score (NES). Gene sets with a false discovery rate (FDR) <0.01 were considered to be significantly enriched.

## Tissue Specimen and Clinical Data Collection

This study was approved by the First Affiliated Hospital of Zhengzhou University. A total of 115 paired CRC tissues and matched adjacent non-tumor tissues were obtained from patients who underwent surgical resection at The First Affiliated Hospital of Zhengzhou University. None of the patients received any preoperative chemotherapy or radiotherapy. Written informed consent was obtained from all the patients. The inclusion criteria were as follows: no preoperative chemotherapy, radiotherapy, or targeted therapy; no other types of tumors; and no autoimmune diseases. The specimens obtained during surgery were immediately snap frozen in liquid nitrogen and stored at -80°C until RNA extraction. Clinical staging of the specimens was based on the NCCN (2019) guidelines. This study has passed the ethical review with the number of 2019-KY-423.

## RNA Extraction and Reverse Transcription

Total RNA was isolated from CRC tissues, paired adjacent noncancerous tissues, and CRC cells with RNAiso Plus reagent (Takara, Dalian, China), according to the manufacturer's instructions. The RNA quality was evaluated using a NanoDrop One C (Waltham, MA, USA), and the RNA integrity was assessed using agarose gel electrophoresis. An aliquot of 1 µg of total RNA was reverse-transcribed into complementary DNA (cDNA) using a High-Capacity cDNA Reverse Transcription Kit (TaKaRa Bio, Japan), according to the manufacturer's protocol.

## Quantitative Real-Time PCR

Quantitative real-time PCR (qRT-PCR) was performed using SYBR Assay I Low ROX (Eurogentec, USA) and SYBR® Green PCR Master Mix (Yeason, Shanghai, China) to detect gene expression. The  $2^{-\Delta\Delta C_t}$  method was used to calculate the relative levels of gene expression. The primers are listed in **Supplementary Table S2**. GAPDH was used as the endogenous control for normalization. qRT-PCR assays were performed in triplicate with the following conditions: (1) 95°C for 5 min and (2) 40 cycles of 95°C for 10 s and 60°C for 30 s. The relative expression of genes was calculated using the  $\Delta C_t$  (Ct mRNA-Ct GAPDH) method. The sequences of qRT-PCR primers are listed in **Supplementary Table S2**.

## Statistical Analysis

Independent sample t test and paired t test were utilized to compare the gene expression difference in public data sets and 115 paired tissues, respectively. Differentially expressed analysis was performed by limma package. The Kaplan–Meier method and the log-rank test were used to estimate the different OS between high-risk and low-risk groups. Univariate Cox regression analysis was used to calculate the hazard ratios (HRs). The receiver operating characteristic (ROC) curves were plotted by timeROC package. The area under the ROC curve

(AUC) for survival variable was conducted by the R package timeROC. The R package rms was applied to plot calibration curves. All *p*-values were two-sided, with *p* < 0.05 as statistically significant. The adjusted *p*-value was obtained by Benjamini–Hochberg (BH) multiple-test correction. All data processing, statistical analysis, and plotting were conducted in R 4.0.2 software.

## RESULTS

### Identification of Redox-Associated Genes in CRC

The flow diagram of the data process and analysis is depicted in **Figure 1**. With “REDOX” as the keyword, we searched in the Molecular Signatures Database (MSigDB) [<http://www.gsea-msigdb.org/gsea/msigdb/index.jsp>], and generated 11 relevant pathways. These 11 pathways contained 309 genes, of which a total of 298 could be detected in the TCGA and GEO data. Subsequently, we investigated whether these 11 pathways were functionally different between the normal group and tumor group in TCGA–CRC. GSEA analysis showed that the majority of redox-related pathway was dysregulated in CRC (**Figure 2A**). Subsequently, the different expression analysis was performed according to the redox-related genes. In total, we identified 118 differentially expressed genes (DEGs) (**Figure 2B**). Univariate Cox analysis revealed 17 prognostically relevant genes among these 118 genes (**Figure 2C**).

### Construction and Evaluation of the RDPS

The 17 OS-associated genes were selected to construct an RDPS based on the LASSO Cox regression model. We identified eight genes that were strongly predictive of OS (**Figures 3A, B**). Then, in a penalized COX model, we obtained the optimal lambda value (0.145178). Based on this lambda value, the risk score of RDPS was calculated using the formula weighted by the regression coefficient containing two redox-related genes as follows: risk score = -0.122 \* expression of ADH5 - 0.070 \* expression of HADH. We calculated the risk score of each patient based on this formula. In all four cohorts, OS was shorter in the high-risk group than in the low-risk group (log-rank test, all *p* < 0.05; **Figures 3C–F**). In addition, after controlling for age, sex, TNM stage, AJCC stage, venous invasion, and microsatellite state, the RDPS remained an independent factor with notably prognostic significance (log-rank test, *p* < 0.05; **Figures 4A–D**).

### RDPS Was Well Validated in Four Cohorts and Could Be Used as a CRC Recurrence Risk Assessment Factor

The ROC curve and calibration plot were utilized to evaluate the accuracy and calibration of RDPS, respectively. In training set TCGA–CRC, the AUCs for predicting OS at 1, 3, and 5 years were 0.725, 0.712, and 0.741. In three public validation cohorts, the AUCs for predicting OS at 1, 3, and 5 years were as follows: 0.720, 0.707, and 0.704 in GSE17536; 0.893, 0.731, and 0.764 in

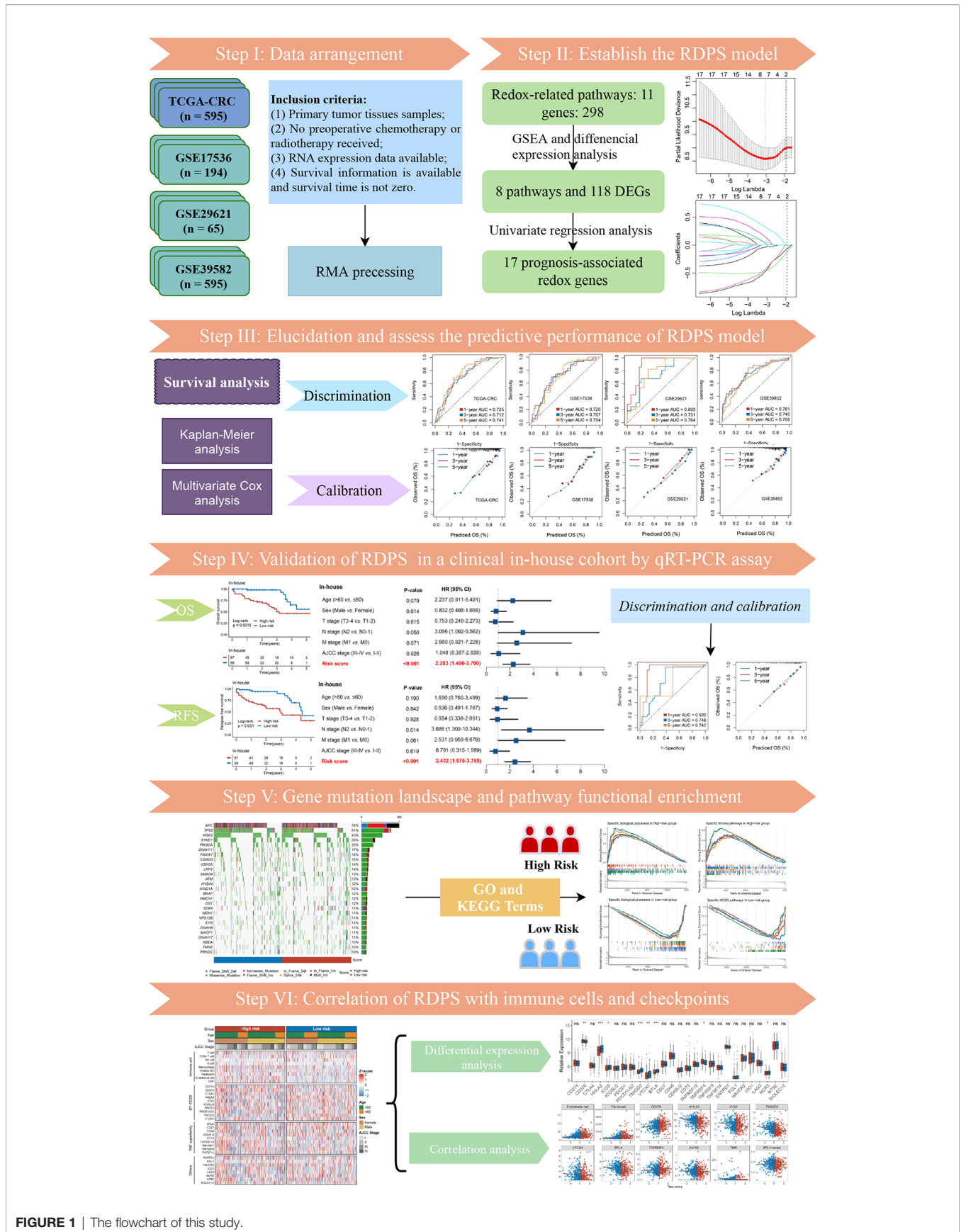


**FIGURE 1 |** The flowchart of this study.

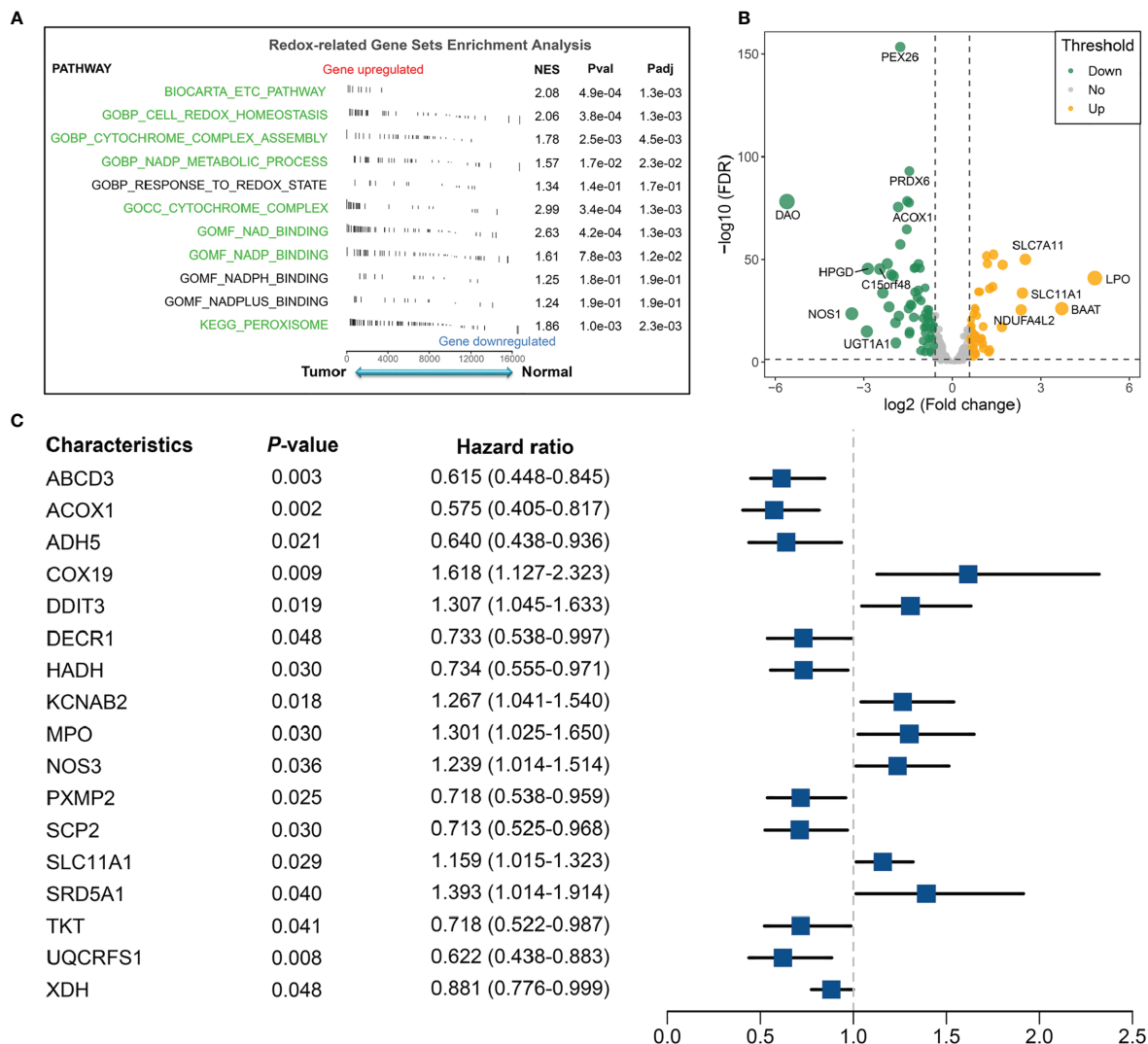


**FIGURE 2** | Identification of redox-associated pathways and genes between the normal group and tumor group in the TCGA-CRC cohort. **(A)** Redox-related gene set enrichment analysis in the normal and tumor groups. **(B)** Differential analysis of redox-related genes in TCGA-CRC. **(C)** Univariate Cox regression revealed 17 redox-related genes with significant prognostic significance.

GSE29621; and 0.761, 0.740, and 0.708 in GSE39582 (Figures 5A–D). Additionally, the calibration plot revealed that RDPS showed a remarkable correction effect with a predicted OS probability of 1, 3, or 5 years, accurately describing the true risk observed in all four cohorts (Figures 5E–H). In short, RDPS represents high predictive accuracy for predicting prognosis in CRC patients. In order to compare our RDPS model with published metabolism-related signatures, we applied the compareC R package to compare the performance among these signatures (28–32). As illustrated in Figure S1, our RDPS model ranked first in the predictive power in TCGA-CRC, GSE17536, and GSE29621. Of note, RDPS ranked second in GSE39582, weaker than Liu’s model, which might be because Liu’s model was developed in GSE39582. Indeed, Liu’s model did not perform well in other validation datasets. Overall, our RDPS model displayed

more stable performance. Since the recurrence of CRC is a key factor for determining the prognosis of patients, we further evaluated the predictive ability of RDPS for CRC recurrence. Likewise, the results of Kaplan–Meier analysis and multivariate Cox regression analysis in the four cohorts showed that the high-risk group possesses adverse recurrence-free survival (RFS) (Figures 6A–D), and risk score was an independent risk factor for RFS (Figures 6E–H).

### Validation of RDPS in a Clinical In-House Cohort

Furthermore, we performed qRT-PCR assays in a clinical cohort containing 115 CRC patients. Clinical information of the 115 cases is illustrated in Supplementary Table S1. Kaplan–Meier analysis concluded that there was a dramatically statistical

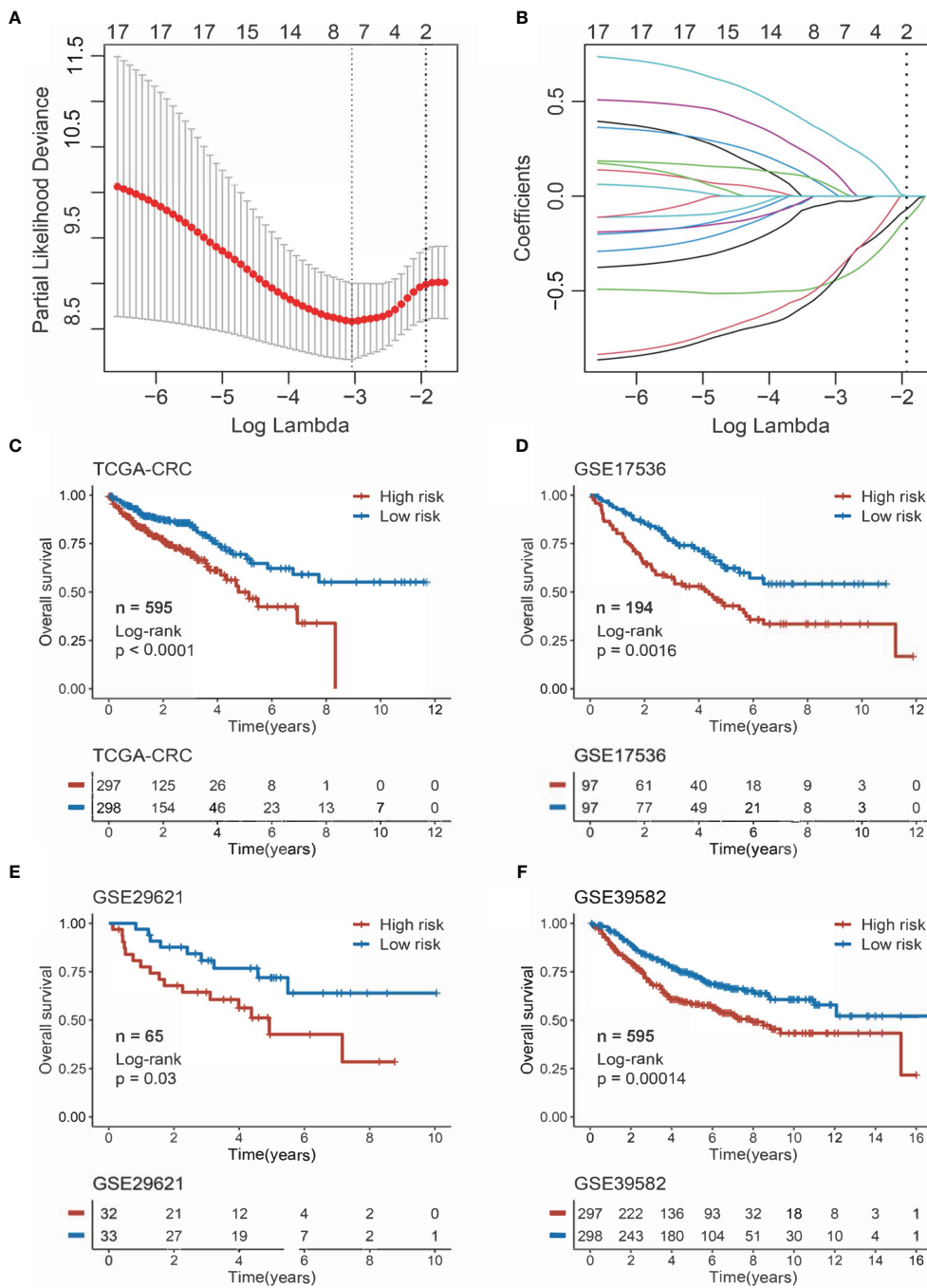


**FIGURE 3** | Construction and evaluation of RDPS. **(A)** Ten-time cross-validations to tune the parameter selection in the LASSO model. The two dotted vertical lines are drawn at the optimal values by minimum criteria (left) and 1-SE criteria (right). **(B)** LASSO coefficient profiles of the candidate genes for risk score construction. **(C-F)** Kaplan-Meier curves for OS according to the risk score in four cohorts.

difference in OS and RFS between the high- and low-risk groups (**Figures 7A, B**). Multivariate Cox regression analysis showed that the risk score calculated from the RDPS model remains statistically significant and acts as a stable independent risk factor for OS (HR: 2.283 [1.408–3.700],  $p < 0.001$ ) and RFS (HR: 2.432 [1.575–3.755],  $p < 0.001$ ) (**Figures 7C, D**), after adjusting for

underlying confounding factors (including age, sex, T, N, M, and AJCC stage). The time-dependent ROC analysis revealed adequate precision and good repeatability of RDPS: the AUCs of predicting OS at 1, 3, and 5 years were 0.920, 0.748, and 0.742, respectively (**Figure 7E**). The calibration plot further displayed the predicted probabilities of OS at 1, 3, and 5 years, accurately

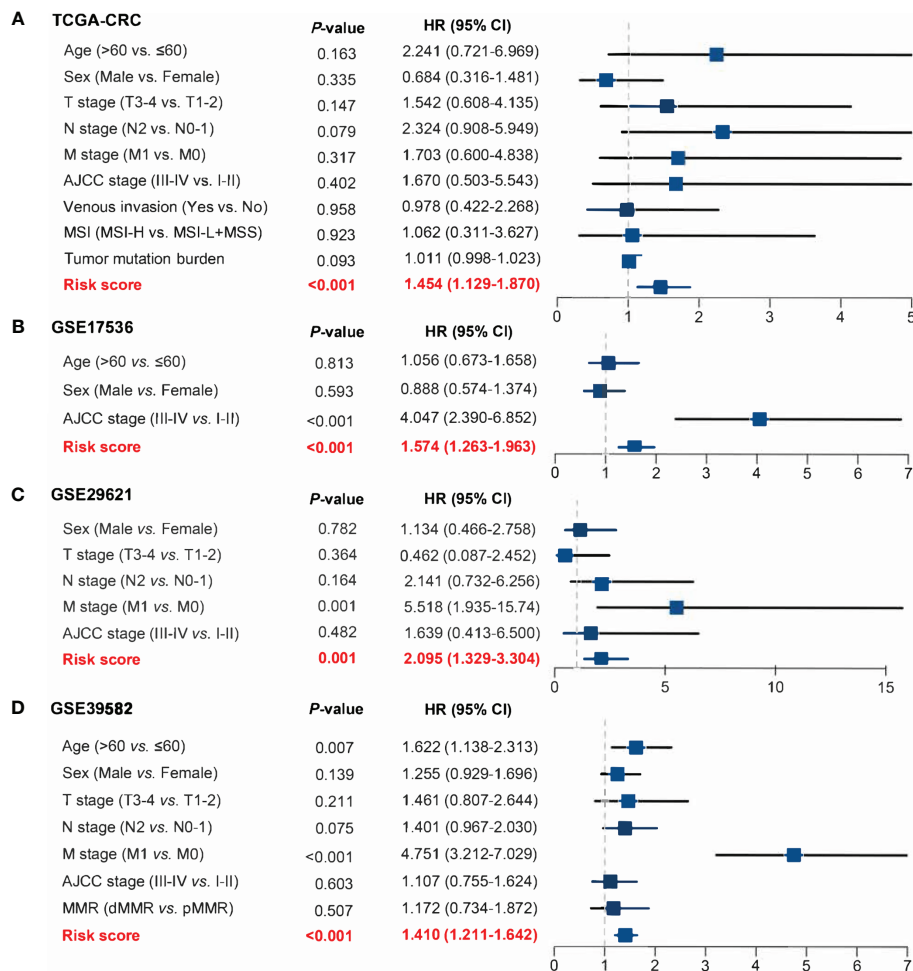


**FIGURE 4** | Power of RDPS in multivariate Cox regression analysis in CRC patients. The risk score was an independent risk factor for prognosis in TCGA-CRC (A), GSE17536 (B), GSE29621 (C), and GSE39582 (D) cohorts.

describing the true risk observed (Figure 7F). On the whole, the consequence from the clinical in-house cohort supported our founding and the public cohort deductions, which favored and elucidated that the RDPS model was considerably steady and could serve as an independent predictor for survival (including OS and RFS) in CRC patients. Furthermore, we also found that our RDPS model performed independent of patients with or without chemotherapy (Figure S2).

## Landscape of Gene Mutations in CRC

The mutational landscape of RDPS was delineated (Figure 8A). Moreover, we investigated the mutation frequencies of driver genes in two groups. It was found that the TP53 mutation frequency was significantly upregulated and the mutation frequencies of PIK3CA, SOX9, and MDN1 were significantly downregulated in the high-risk group compared with the low-risk group (Figure 8B). APC, TP53, and KRAS were the most commonly mutated genes in both high- and low-risk groups, independently. This suggests that the high mutation frequency of these three genes is an important factor

leading to CRC (Figure 8B). Considering that copy number alteration (CNA) mainly includes amplification (AMP) and homozygous deletion (HOMDEL), we analyzed CNA in patients at different risk levels. We found that in the high-risk group, URAD, SERINC3, PKIG, PDX1, OSER1, and LINC00543 were significantly amplified; significant deletions were RBFOX1, WWOX, CCSER1, CSMD1, and AGLB4. However, in the low-risk group, TPS2, REM1, LINC00028, ID1, HM13, and DEFB124 were significantly amplified; significant deletions were found for RBFOX1, WWOX, MACROD2, CCSER1, and CSMD1. Both amplified and homozygously deleted fragments hardly coincide in the high- and low-risk groups, especially in terms of AMP (Figure 8C).

## Inflammation Landscape and Immune Checkpoint Profiles of RDPS

In GO and KEGG analyses, the pathways significantly enriched in the high-risk group were all shown to be closely related to epithelial-mesenchymal transition (EMT), involving the cytoskeleton, intercellular junctions, and cell differentiation processes, such as

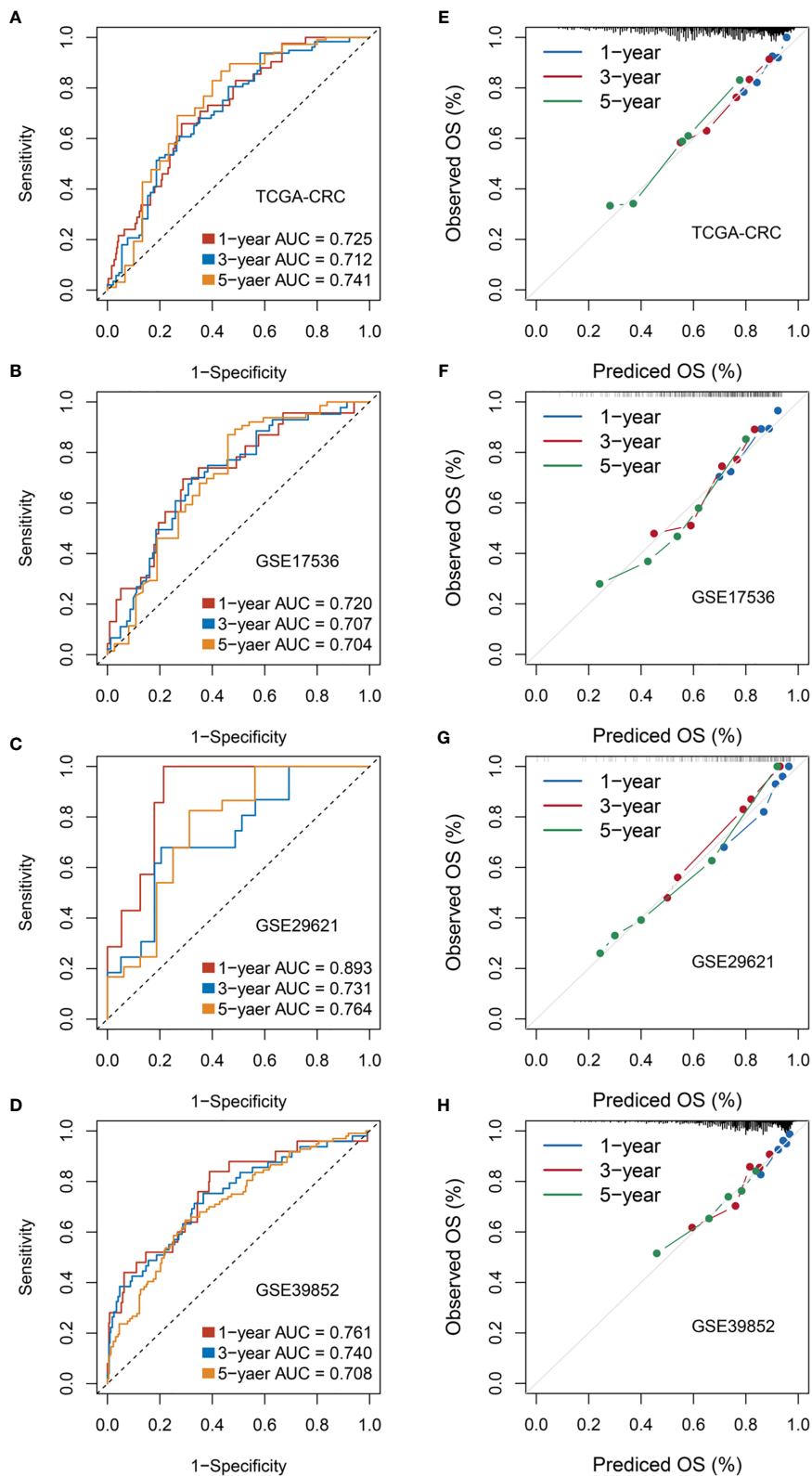


**FIGURE 5** | Evaluation of RDPS in predicting OS in four cohorts. **(A–D)** Time-dependent ROC analysis for predicting OS at 1, 3, and 5 years. **(E–H)** Calibration plots for comparing the actual probabilities and the predicted probabilities of OS at 1, 3, and 5 years.



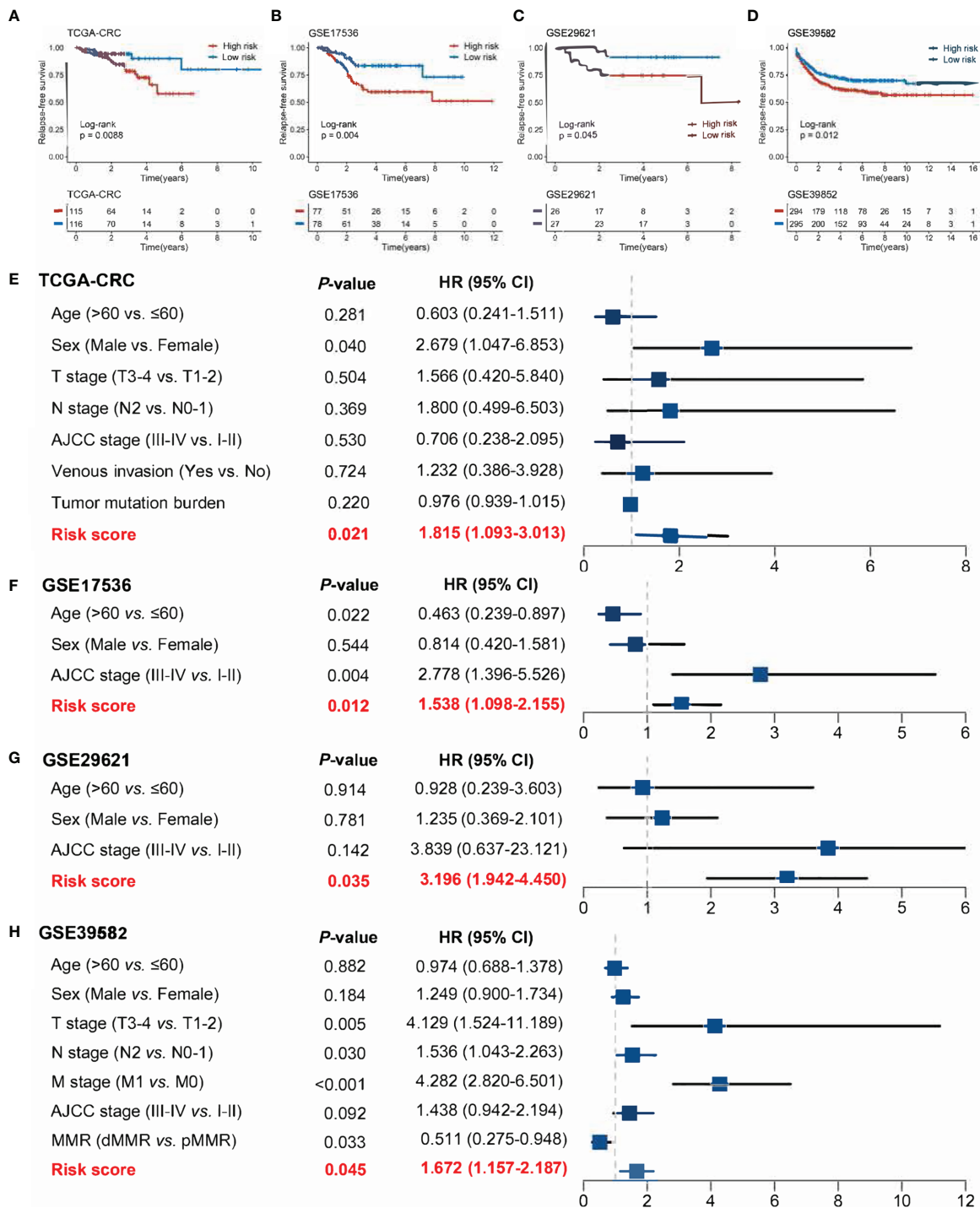


**FIGURE 6** | Evaluation of the ability of risk scores to predict CRC recurrence in four public cohorts. (A–D) Kaplan–Meier curves of RFS according to the RDPS model in four cohorts. (E–H) Multivariate Cox regression analysis of the risk score in four cohorts.

chondrocyte differentiation, collagen fibril organization, extracellular matrix organization, calcium signaling pathway, cell adhesion molecules, and ECM–receptor interactions (Figures 9A, C). Of note, the consistency of low risk is related to the related enzyme

and electron chain transport processes in the redox process, such as ATP synthesis-coupled electron transport, mitochondrial translation, NADH dehydrogenase complex assembly, pentose and glucuronate interconversions, and pyruvate metabolism

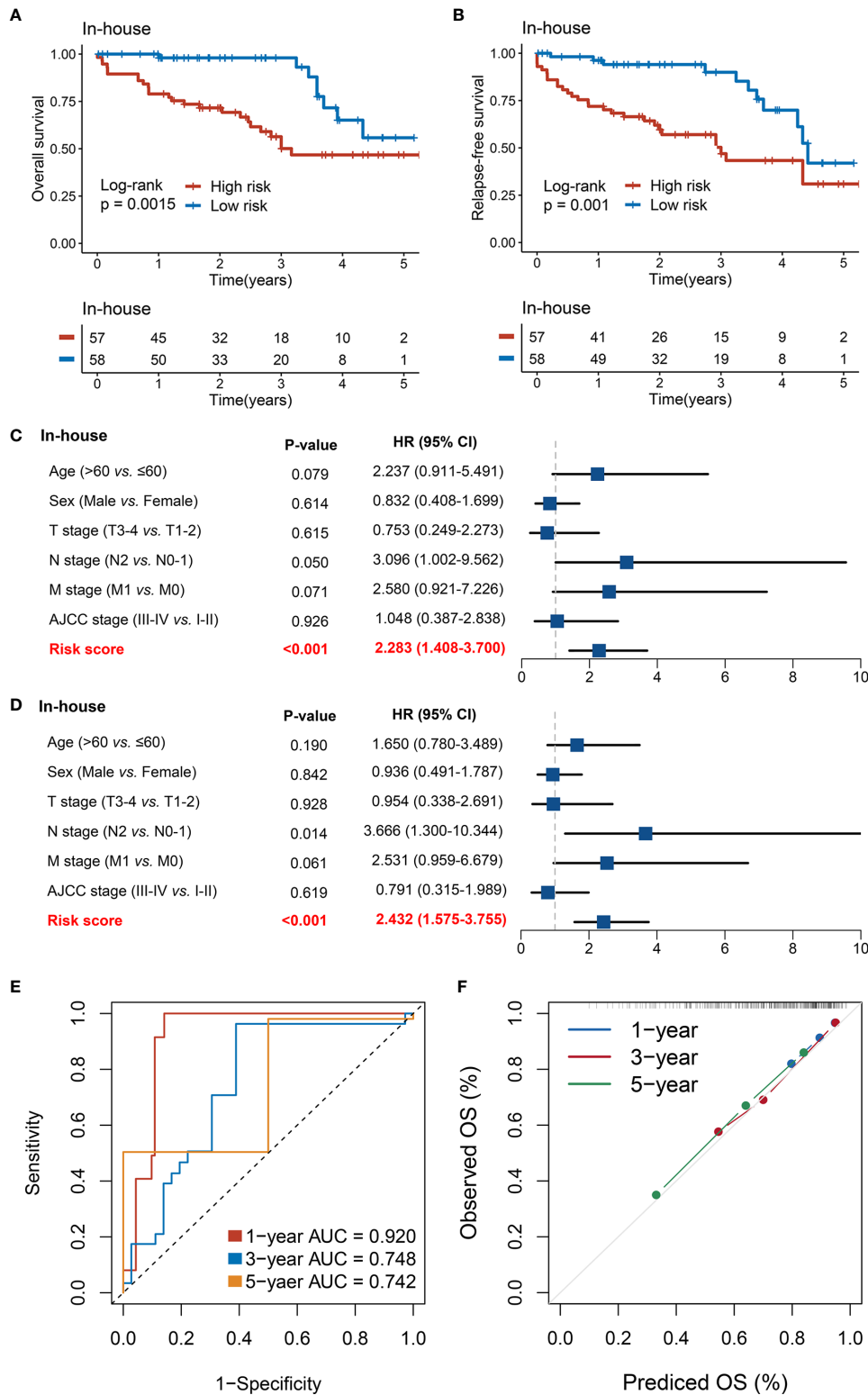


**FIGURE 7** | Validation of our discovery in a clinical in-house cohort. **(A, B)** Kaplan-Meier curves of OS **(A)** and RFS **(B)** according to the RDPS. **(C, D)** Multivariate Cox regression analysis of the risk score for OS **(C)** and RFS **(D)**. **(E)** Time-dependent ROC analysis for predicting RFS at 1, 3, and 5 years. **(F)** Calibration plots for comparing the actual probabilities and the predicted probabilities of OS at 1, 3, and 5 years.

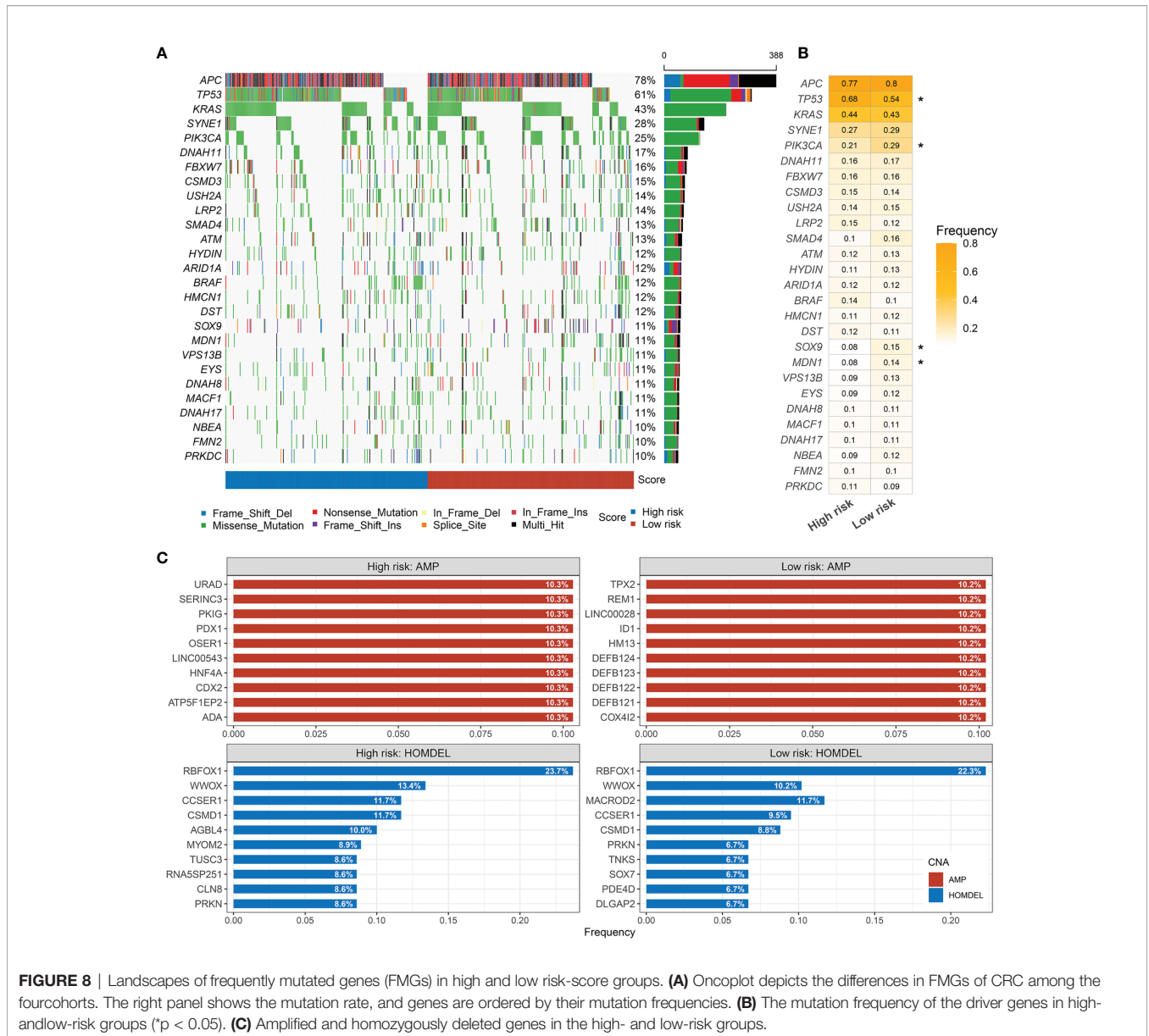


**FIGURE 8** | Landscapes of frequently mutated genes (FMGs) in high and low-risk-score groups. **(A)** Oncoplot depicts the differences in FMGs of CRC among the fourcohorts. The right panel shows the mutation rate, and genes are ordered by their mutation frequencies. **(B)** The mutation frequency of the driver genes in high-andlow-risk groups (\*p < 0.05). **(C)** Amplified and homozygously deleted genes in the high- and low-risk groups.

(**Figures 9B, D**). Immune infiltration in the tumor microenvironment has been shown to play a critical role in the development and progression of tumors and affects the clinical prognosis of cancer patients. We found that the landscape characteristics of the high-risk group were different from those of the low-risk group. The immune landscape is shown in **Figure 10A**. We analyzed the abundance of nine immune cells in tissues with different risk fractions and found that the infiltration abundance of T cells, endothelial cells, and cancer-associated fibroblasts (CAFs) was significantly richer in the high-risk group (**Figure 10B**). In addition, we observed that CD276 and TNFRSF4 were upregulated in the low-risk group, while HHLA2, ICOS, TMIGD2, VTCN1, BTLA, and NCR3 were significantly overexpressed in the high-risk group (**Figure 10C**). Patients in the high-risk group processed a lower tumor mutation burden (TMB)

and immunophenoscore (IPS) (**Figures 10D, E**), which suggested a weak immunogenicity in the high-risk group relative to the low-risk group. Additionally, cells or immune checkpoints with disparate abundance or expression were selected for correlation with risk score, and the results were as expected (**Figure 10F**). These results indicate that there may be an intimate correlation between the RDPS model and the infiltration of some immune cells and the expression of immune checkpoints.

## DISCUSSION

Recently, the modulation of redox-related pathways and targets has been shown to stimulate multiple signaling pathways to mediate the malignant phenotype of cancer, which involves cell-

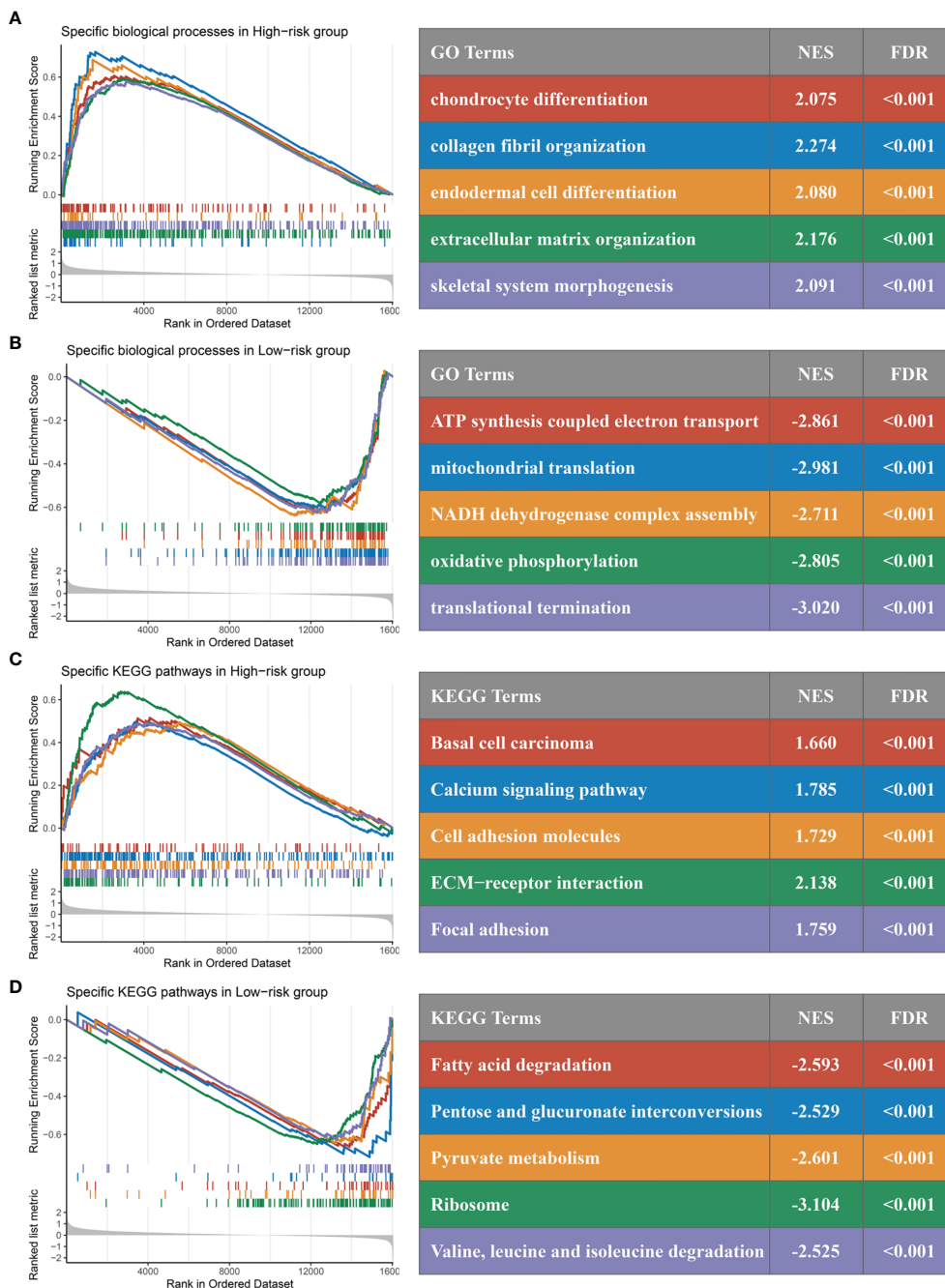


**FIGURE 9 |** GSEA functional pathway analysis. **(A, B)** Significantly enriched Gene Ontology terms between high **(A)** and low **(B)** risk groups. **(C, D)** Significantly enriched Kyoto Encyclopedia of Genes and Genomes terms between high **(C)** and low **(D)** risk groups.

specific death (33), treatment sensitivity (24), proliferation, invasiveness, and angiogenesis (34). In this study, we first screened and summarized 11 redox-related pathways and performed a functional difference analysis between the tumor and normal groups in TCGA-CRC. As a result, we found that the majority of redox-related pathways were dysregulated in CRC, which suggested that the redox-related pathways might play vital

roles in the initiation and progression of CRC. Further, based on the expression profiles of redox-related genes, we established and validated a two-gene signature for evaluating the prognosis of CRC. This signature includes two genes: ADH5 and HADH. Members of the alcohol dehydrogenase family metabolize a wide variety of substrates. Digenic mutation in ADH5 and ALDH2 impairs formaldehyde clearance and causes a multisystem

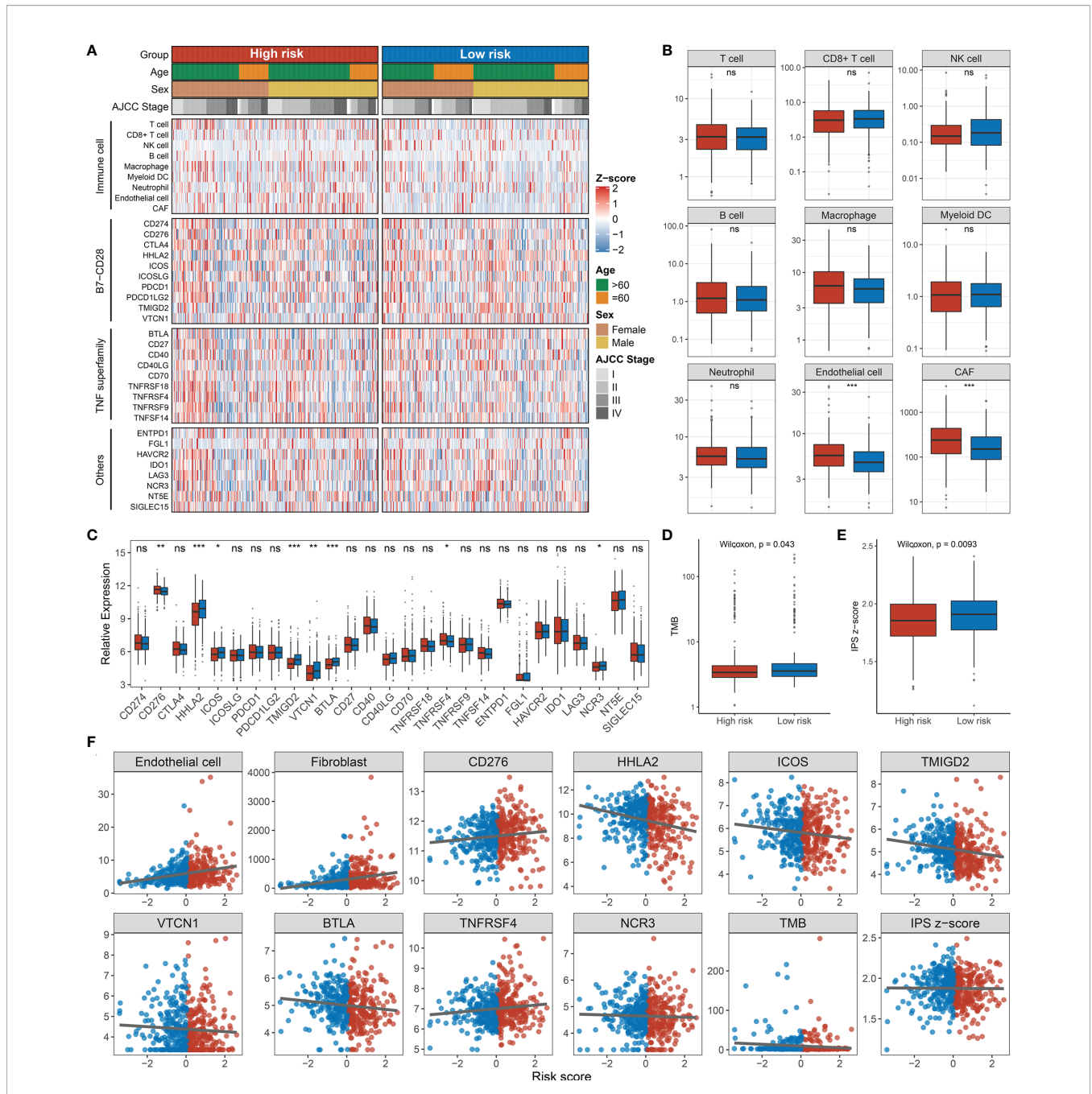


**FIGURE 10 |** Immune infiltration analysis. **(A)** Assessment of infiltration abundance of nine immune cells and 27 immune checkpoints in patients with high or low RDPS scores. **(B)** Abundance of immune cell infiltrates in the high- and low-risk groups. **(C)** Differential expression analysis of immune checkpoints. The difference of TMB **(D)** and IPS **(E)** in different risk groups. **(F)** Correlation analysis of immune cells or checkpoints with risk scores (ns,  $p > 0.05$ ; \* $p < 0.05$ ; \*\* $p < 0.01$ ; \*\*\* $p < 0.001$ ). NS, none significance.

disorder (35). Animal experiments confirmed that mice lacking ADH5 and ALDH2 have greatly shortened lifespans and develop leukemia *in vivo* (36). HADH, as one of the target genes of the Wnt pathway, has been shown to be involved in regulating the growth and proliferation of CRC cells (37). Therefore, ADH5 and HADH were likely to have a latent role in the malignant biological behavior of CRC.

CRC, a highly heterogeneous malignancy, is a fatal health problem threatening the world (38, 39). Strikingly, Ji et al. argued that controlling the metabolic patterns of cancer stem cells is an innovative therapeutic strategy for CRC patients with adverse prognosis and relapse (19). We calculated and grouped the risk score of each patient and found that the high-risk group had a worse outcome, using the Kaplan–Meier method, in four public

cohorts. Subsequently, multivariate analysis suggested that the RDPS risk score could act as an independent poor predictive factor for survival in CRC patients. Moreover, the predictive ability of RDPS was estimated by ROC, wherein the 1-year prediction discrimination was 0.893 and the 1-, 3-, and 5-year AUC were all greater than 0.7 in the four public cohorts. The results indicate that the RDPS model has an excellent fitting and prospective predictive ability.

Recurrence and metastasis are dominating causes of death for CRC patients (40, 41). Therefore, we further evaluated the ability of the RDPS to predict CRC recurrence. Similarly, the model exhibited strong predictive power in predicting relapse. Specifically, we demonstrated that the high-risk score predicted unfavorable RFS and that the risk score was an independent risk factor for RFS in CRC patients in four public cohorts, respectively. Furthermore, we shed light on the model in a sample of 115 clinical CRC patients. Notably, patients in the low-risk score group had longer OS and RFS compared with the high-risk group. In multivariate analysis, the risk score played a stable and independent risk factor for survival. Likewise, the accuracy and power of the model are good. The inclusion and validation of clinical cohorts suggested that RDPS models have potential clinical prospects in the prediction of metastasis and prognosis in CRC patients, which could contribute to the implementation of clinical decision-making.

Generally, similar links exist between landscape diversity and landscape function. In our analysis, gene mutation frequencies, amplifications, and homozygous deletions were not identical in the mutant landscape of the high-risk group, suggesting that there were differences between the high- and low-risk groups in gene levels. Interestingly, the mutation frequency of TP53 was significantly frequent in the high-risk group. It is well-known that p53 is a target of drugs such as cetuximab and affects the sensitivity of chemotherapeutic drugs such as oxaliplatin (42, 43). In mechanism, the p53 protein mediates multiple signaling pathways such as cell proliferation, apoptosis, and cancer stem cells (44–46). This suggests that high-risk patients selected by the RDPS model may be more likely to show malignant phenotypes such as proliferation, metastasis, and drug resistance. Accordingly, we found relevant evidence in the GSEA pathway enrichment analysis. The significantly enriched pathways in the high-risk group were mainly significantly related to cell migration, such as collagen fiber structure, extracellular matrix tissue, and calcium signaling pathway, suggesting that it may cause cell metastasis and spread. However, the low-risk group was mainly enriched in redox and energy metabolism-related pathways, suggesting that redox reactions may play a fundamental role in it.

Recently, the therapeutic regimen of combined immunotherapy has led to a significant improvement in the efficacy of CRC (47, 48). In addition, there is an intimate association between redox and immune responses. As proof, the glucose-6-phosphate dehydrogenase–NADPH redox system indirectly activated T cells and advances alleviate T cell hypofunction in the tumor microenvironment (49). Fat oxidation has been implicated in tumor local infiltration and function of CD8+ T cells (50). Conversely, tumor-induced neutrophils participate

in mitochondrial metabolism ultimately causing immunosuppressive effects, suggesting that the immune system could also mediate redox-related mechanisms to affect immunity (51). In order to investigate whether the RDPS model is helpful for the study of clinical immunotherapy regimens, we explored the association between risk scores and immune cells and checkpoints. Endothelial cells and CAFs are abundant in the high-risk group. Endothelial cells are important regulators of tumor metastasis propagation (52). The differentially expressed immune checkpoints derived from the analysis are also providing us with promising immunotherapeutic targets. We observed that the high-risk group possesses lower TMB and IPS, suggesting that high-risk patients had reduced local tumor-specific neoantigen production and that the immune response capacity may be in a weaker state compared with the low-risk group.

Our study proposes a novel perspective to match signatures from redox-driven genes and establish prediction models, which predicts the prognosis and recurrence of CRC. Moreover, the risk score was inversely associated with local immunogenicity. Furthermore, we performed RNA-level validation in collected clinical cohorts. Nevertheless, limited by the lack of data, our algorithm only takes into account the heterogeneity of patients and did not attain spatiotemporal heterogeneity within tumors. Second, despite the validation of gene expression at the RNA level, further exploration regarding the mechanisms of *in vivo* experiments in cells or animals would make the findings more convincing.

Summarizing the above, our study identifies and validates a predictive model consisting of two redox-driven implicated gene signatures. The RDPS model predicted OS and RFS well in four public cohorts and one clinical cohort of CRC and was an independent risk factor for survival. In addition, the differences in immune cells and related checkpoints suggest that there is an intimate association between redox and immune cells or checkpoints, which may provide promising predictors and immunotherapy targets for CRC patients.

## DATA AVAILABILITY STATEMENT

The datasets presented in this study can be found in online repositories. The names of the repository/repositories and accession number(s) can be found in the article/**Supplementary Material**.

## ETHICS STATEMENT

The studies involving human participants were reviewed and approved by the Ethics Committee of the First Affiliated Hospital of Zhengzhou University. The patients/participants provided their written informed consent to participate in this study. Written informed consent was obtained from the individual(s) for the publication of any potentially identifiable images or data included in this article.

## AUTHOR CONTRIBUTIONS

QD made the conceptualization. ZS, ZL, and LL were involved in the methodology. ZS, LL, SH, and ZC provided the resources. QD and ZL analyzed the data. QD, ZL and LM prepared the original draft. QD, ZL and XH reviewed and edited the manuscript. XH, JH, GW, and WY supervised the study. All authors contributed to the article and approved the submitted version.

## FUNDING

This study was supported by the National Natural Science Foundation of China (Grant Nos. 81972663, U2004112); Key Scientific Research Projects of Institutions of Higher Education in Henan Province (Grant No. 19A310024); the National Natural Science Foundation of Henan Province (Grant No. 212300410074); Science and Technology Project of Henan Provincial Department of Education (Grant No. 21A320036);

## REFERENCES

- Ladabaum U, Dominitz JA, Kahi C, Schoen RE. Strategies for Colorectal Cancer Screening. *Gastroenterology* (2020) 158(2):418–32. doi: 10.1053/j.gastro.2019.06.043
- Arnold M, Sierra MS, Laversanne M, Soerjomataram I, Jemal A, Bray F. Global Patterns and Trends in Colorectal Cancer Incidence and Mortality. *Gut* (2017) 66(4):683–91. doi: 10.1136/gutjnl-2015-310912
- Collaborative R, Zaborowski AM, Abdile A, Adamina M, Aigner F, d'Allens L, et al. Characteristics of Early-Onset vs Late-Onset Colorectal Cancer: A Review. *JAMA Surg* (2021) 156(9):865–74. doi: 10.1001/jamasurg.2021.2380
- McCarthy B, Cudykier A, Singh R, Levi-Polyachenko N, Soker S. Semiconducting Polymer Nanoparticles for Photothermal Ablation of Colorectal Cancer Organoids. *Sci Rep* (2021) 11(1):1532. doi: 10.1038/s41598-021-81122-w
- Ou J, Peng Y, Yang W, Zhang Y, Hao J, Li F, et al. ABHD5 Blunts the Sensitivity of Colorectal Cancer to Fluorouracil via Promoting Autophagic Uricil Yield. *Nat Commun* (2019) 10(1):1078. doi: 10.1038/s41467-019-08902-x
- Ijaz K, Kasowski E, Arthur RR, Angulo FJ, Dowell SF. International Health Regulations—what Gets Measured Gets Done. *Emerg Infect Dis* (2012) 18(7):1054–7. doi: 10.3201/eid1807.120487
- Hunter P. The Fourth Pillar: Despite Some Setbacks in the Clinic, Immunotherapy has Made Notable Progress Toward Becoming an Additional Therapeutic Option Against Cancer. *EMBO Rep* (2017) 18(11):1889–92. doi: 10.15252/embr.201745172
- Aris M, Barrio MM. Combining Immunotherapy With Oncogene-Targeted Therapy: A New Road for Melanoma Treatment. *Front Immunol* (2015) 6:46. doi: 10.3389/fimmu.2015.00046
- Dunn GP, Cloughesy TF, Maus MV, Prins RM, Reardon DA, Sonabend AM. Emerging Immunotherapies for Malignant Glioma: From Immunogenomics to Cell Therapy. *Neuro Oncol* (2020) 22(10):1425–38. doi: 10.1093/neuonc/noaa154
- Ding Y, Yu J, Chen X, Wang S, Tu Z, Shen G, et al. Dose-Dependent Carbon-Dot-Induced ROS Promote Uveal Melanoma Cell Tumorigenicity via Activation of mTOR Signaling and Glutamine Metabolism. *Adv Sci (Weinh)* (2021) 8(8):2002404. doi: 10.1002/advs.202002404
- Bose C, Alves I, Singh P, Palade PT, Carvalho E, Borsheim E, et al. Sulforaphane Prevents Age-Associated Cardiac and Muscular Dysfunction Through Nrf2 Signaling. *Aging Cell* (2020) 19(11):e13261. doi: 10.1111/acel.13261
- Perez-Perez ME, Zaffagnini M, Marchand CH, Crespo JL, Lemaire SD. The Yeast Autophagy Protease Atg4 Is Regulated by Thioredoxin. *Autophagy* (2014) 10(11):1953–64. doi: 10.4161/auto.34396
- Basak D, Uddin MN, Hancock J. The Role of Oxidative Stress and Its Counteractive Utility in Colorectal Cancer (CRC). *Cancers (Basel)* (2020) 12(11):3336. doi: 10.3390/cancers12113336
- Ju HQ, Lu YX, Chen DL, Zuo ZX, Liu ZX, Wu QN, et al. Modulation of Redox Homeostasis by Inhibition of MTHFD2 in Colorectal Cancer: Mechanisms

and Therapeutic Implications. *J Natl Cancer Inst* (2019) 111(6):584–96. doi: 10.1093/jnci/djy160

15. Xu J, Ji L, Ruan Y, Wan Z, Lin Z, Xia S, et al. UBQLN1 Mediates Sorafenib Resistance Through Regulating Mitochondrial Biogenesis and ROS Homeostasis by Targeting PGC1beta in Hepatocellular Carcinoma. *Signal Transduct Target Ther* (2021) 6(1):190. doi: 10.1038/s41392-021-00594-4

16. Bull CJ, Bell JA, Murphy N, Sanderson E, Davey Smith G, Timpson NJ, et al. Adiposity, Metabolites, and Colorectal Cancer Risk: Mendelian Randomization Study. *BMC Med* (2020) 18(1):396. doi: 10.1186/s12916-020-01855-9

17. Guinter MA, McCullough ML, Gapstur SM, Campbell PT. Associations of Pre- and Postdiagnosis Diet Quality With Risk of Mortality Among Men and Women With Colorectal Cancer. *J Clin Oncol* (2018) 36(34):JCO1800714. doi: 10.1200/JCO.18.00714

18. Kitahara CM, Berndt SI, de Gonzalez AB, Coleman HG, Schoen RE, Hayes RB, et al. Prospective Investigation of Body Mass Index, Colorectal Adenoma, and Colorectal Cancer in the Prostate, Lung, Colorectal, and Ovarian Cancer Screening Trial. *J Clin Oncol* (2013) 31(19):2450–9. doi: 10.1200/JCO.2012.48.4691

19. Ji Y, Yang C, Tang Z, Yang Y, Tian Y, Yao H, et al. Adenylate Kinase hCINAP Determines Self-Renewal of Colorectal Cancer Stem Cells by Facilitating LDHA Phosphorylation. *Nat Commun* (2017) 8:15308. doi: 10.1038/ncomms15308

20. Shashni B, Nishikawa Y, Nagasaki Y. Management of Tumor Growth and Angiogenesis in Triple-Negative Breast Cancer by Using Redox Nanoparticles. *Biomaterials* (2021) 269:120645. doi: 10.1016/j.biomaterials.2020.120645

21. Jones N, Blagih J, Zani F, Rees A, Hill DG, Jenkins BJ, et al. Fructose Reprogrammes Glutamine-Dependent Oxidative Metabolism to Support LPS-Induced Inflammation. *Nat Commun* (2021) 12(1):1209. doi: 10.1038/s41467-021-21461-4

22. Oliveira MF, Medeiros RCA, Mietto BS, Calvo TL, Mendonca APM, Rosa T, et al. Reduction of Host Cell Mitochondrial Activity as Mycobacterium Leprae's Strategy to Evade Host Innate Immunity. *Immunol Rev* (2021) 301(1):193–208. doi: 10.1111/imr.12962

23. Wei L, Zhao Y, Hu X, Tang L. Redox-Responsive Polycondensate Neoepitope for Enhanced Personalized Cancer Vaccine. *ACS Cent Sci* (2020) 6(3):404–12. doi: 10.1021/acscentsci.9b01174

24. Liu Z, Wang L, Liu L, Lu T, Jiao D, Sun Y, et al. The Identification and Validation of Two Heterogenous Subtypes and a Risk Signature Based on Ferroptosis in Hepatocellular Carcinoma. *Front Oncol* (2021) 11:619242. doi: 10.3389/fonc.2021.619242

25. Liu Z, Zhang Y, Dang Q, Wu K, Jiao D, Li Z, et al. Genomic Alteration Characterization in Colorectal Cancer Identifies a Prognostic and Metastasis Biomarker: FAM83A|Ido1. *Front Oncol* (2021) 11:632430. doi: 10.3389/fonc.2021.632430

## SUPPLEMENTARY MATERIAL

The Supplementary Material for this article can be found online at: <https://www.frontiersin.org/articles/10.3389/fonc.2021.743703/full#supplementary-material>

**Supplementary Figure 1** | Comparison between RDPS model and published metabolism-related signals.

**Supplementary Figure 2** | RDPS assessment of survival in patients with and without chemotherapy. **(A, B)**, the effect of RDPS on OS in patients receiving **(A)** and without **(B)** chemotherapy. **(C, D)**, the effect of RDPS on RFS in patients receiving **(C)** and without **(D)** chemotherapy.

26. Liu Z, Lu T, Wang Y, Jiao D, Li Z, Wang L, et al. Establishment and Experimental Validation of an Immune miRNA Signature for Assessing Prognosis and Immune Landscape of Patients With Colorectal Cancer. *J Cell Mol Med* (2021) 25(14):6874–86. doi: 10.1111/jcmm.16696
27. Liu Z, Zhang Y, Shi C, Zhou X, Xu K, Jiao D, et al. A Novel Immune Classification Reveals Distinct Immune Escape Mechanism and Genomic Alterations: Implications for Immunotherapy in Hepatocellular Carcinoma. *J Transl Med* (2021) 19(1):5. doi: 10.1186/s12967-020-02697-y
28. Lin D, Fan W, Zhang R, Zhao E, Li P, Zhou W, et al. Molecular Subtype Identification and Prognosis Stratification by a Metabolism-Related Gene Expression Signature in Colorectal Cancer. *J Transl Med* (2021) 19(1):279. doi: 10.1186/s12967-021-02952-w
29. Luo D, Shan Z, Liu Q, Cai S, Li Q, Li X. A Novel Seventeen-Gene Metabolic Signature for Predicting Prognosis in Colon Cancer. *BioMed Res Int* (2020) 2020:4845360. doi: 10.1155/2020/4845360
30. Miao Y, Li Q, Wang J, Quan W, Li C, Yang Y, et al. Prognostic Implications of Metabolism-Associated Gene Signatures in Colorectal Cancer. *PeerJ* (2020) 8:e9847. doi: 10.7717/peerj.9847
31. Yuan Y, Chen J, Wang J, Xu M, Zhang Y, Sun P, et al. Development and Clinical Validation of a Novel 4-Gene Prognostic Signature Predicting Survival in Colorectal Cancer. *Front Oncol* (2020) 10:595. doi: 10.3389/fonc.2020.00595
32. Zou YF, Rong YM, Tan YX, Xiao J, Yu ZL, Chen YF, et al. A Signature of Hypoxia-Related Factors Reveals Functional Dysregulation and Robustly Predicts Clinical Outcomes in Stage I/II Colorectal Cancer Patients. *Cancer Cell Int* (2019) 19:243. doi: 10.1186/s12935-019-0964-1
33. Saneesh Babu PS, Manu PM, Dhanya TJ, Tapas P, Meera RN, Surendran A, et al. Bis(3,5-Diiodo-2,4,6-Trihydroxyphenyl)Squaraine Photodynamic Therapy Disrupts Redox Homeostasis and Induce Mitochondria-Mediated Apoptosis in Human Breast Cancer Cells. *Sci Rep* (2017) 7:42126. doi: 10.1038/srep42126
34. Naczki C, John B, Patel C, Lafferty A, Ghoneum A, Afify H, et al. SPARC Inhibits Metabolic Plasticity in Ovarian Cancer. *Cancers* (2018) 10(10):385. doi: 10.3390/cancers10100385
35. Oka Y, Hamada M, Nakazawa Y, Muramatsu H, Okuno Y, Higasa K, et al. ALDH2-Digenic Mutations in and Impair Formaldehyde Clearance and Cause a Multisystem Disorder, AMeD Syndrome. *Sci Adv* (2020) 6(51):eabd7197. doi: 10.1126/sciadv.abd7197
36. Dingler F, Wang M, Mu A, Millington C, Oberbeck N, Watcham S, et al. Two Aldehyde Clearance Systems Are Essential to Prevent Lethal Formaldehyde Accumulation in Mice and Humans. *Mol Cell* (2020) 80(6):996–1012.e9. doi: 10.1016/j.molcel.2020.10.012
37. Voloshanenko O, Schwartz U, Kranz D, Rauscher B, Linnebacher M, Augustin I, et al.  $\beta$ -Catenin-Independent Regulation of Wnt Target Genes by RoR2 and ATF2/ATF4 in Colon Cancer Cells. *Sci Rep* (2018) 8(1):3178. doi: 10.1038/s41598-018-20641-5
38. Schell MJ, Yang M, Teer JK, Lo FY, Madan A, Coppola D, et al. A Multigene Mutation Classification of 468 Colorectal Cancers Reveals a Prognostic Role for APC. *Nat Commun* (2016) 7:11743. doi: 10.1038/ncomms11743
39. Liu Y, Chen X, Cheng R, Yang F, Yu M, Wang C, et al. The Jun/miR-22/HuR Regulatory Axis Contributes to Tumorigenesis in Colorectal Cancer. *Mol Cancer* (2018) 17(1):11. doi: 10.1186/s12943-017-0751-3
40. Jackstadt R, van Hooff SR, Leach JD, Cortes-Lavaud X, Lohuis JO, Ridgway RA, et al. Epithelial NOTCH Signaling Rewires the Tumor Microenvironment of Colorectal Cancer to Drive Poor-Prognosis Subtypes and Metastasis. *Cancer Cell* (2019) 36(3):319–36.e7. doi: 10.1016/j.ccell.2019.08.003
41. Sanz-Pamplona R, Melas M, Maoz A, Schmit SL, Rennert H, Lejbkowitz F, et al. Lymphocytic Infiltration in Stage II Microsatellite Stable Colorectal Tumors: A Retrospective Prognosis Biomarker Analysis. *PLoS Med* (2020) 17(9):e1003292. doi: 10.1371/journal.pmed.1003292
42. Guo Y, Parry JJ, Laforest R, Rogers BE, Anderson CJ. The Role of P53 in Combination Radioimmunotherapy With  $^{64}\text{Cu}$ -DOTA-Cetuximab and Cisplatin in a Mouse Model of Colorectal Cancer. *J Nucl Med* (2013) 54(9):1621–9. doi: 10.2967/jnumed.112.118539
43. Wilson PM, Fazzino W, LaBonte MJ, Lenz HJ, Ladner RD. Regulation of Human DUTPase Gene Expression and P53-Mediated Transcriptional Repression in Response to Oxaliplatin-Induced DNA Damage. *Nucleic Acids Res* (2009) 37(1):78–95. doi: 10.1093/nar/gkn910
44. Holdt LM, Stahringer A, Sass K, Pichler G, Kulak NA, Wilfert W, et al. Circular Non-Coding RNA ANRIL Modulates Ribosomal RNA Maturation and Atherosclerosis in Humans. *Nat Commun* (2016) 7:12429. doi: 10.1038/ncomms12429
45. Hsu JI, Dayaram T, Tovy A, De Braekeleer E, Jeong M, Wang F, et al. PPM1D Mutations Drive Clonal Hematopoiesis in Response to Cytotoxic Chemotherapy. *Cell Stem Cell* (2018) 23(5):700–13.e6. doi: 10.1016/j.stem.2018.10.004
46. Ihle M, Biber S, Schroeder I, Blattner C, Deniz M, Damia G, et al. Impact of the Interplay Between Stemness Features, P53 and Pol Iota on Replication Pathway Choices. *Nucleic Acids Res* (2021) 49(13):7457–75. doi: 10.1093/nar/gkab526
47. Huang K, Chiang S, Chen W, Chen T, Hu C, Yang P, et al. Decitabine Augments Chemotherapy-Induced PD-L1 Upregulation for PD-L1 Blockade in Colorectal Cancer. *Cancers* (2020) 12(2):462. doi: 10.3390/cancers12020462
48. Sur D, Havasi A, Cainap C, Samasca G, Burz C, Balacescu O, et al. Chimeric Antigen Receptor T-Cell Therapy for Colorectal Cancer. *J Clin Med* (2020) 9(1):182. doi: 10.3390/jcm9010182
49. Gu M, Zhou X, Sohn JH, Zhu L, Jie Z, Yang JY, et al. NF- $\kappa$ B-Inducing Kinase Maintains T Cell Metabolic Fitness in Antitumor Immunity. *Nat Immunol* (2021) 22(2):193–204. doi: 10.1038/s41590-020-00829-6
50. Ringel AE, Drijvers JM, Baker GJ, Catozzi A, Garcia-Canaveras JC, Gassaway BM, et al. Obesity Shapes Metabolism in the Tumor Microenvironment to Suppress Anti-Tumor Immunity. *Cell* (2020) 183(7):1848–66.e26. doi: 10.1016/j.cell.2020.11.009
51. Rice CM, Davies LC, Subleski JJ, Maio N, Gonzalez-Cotto M, Andrews C, et al. Tumour-Elicited Neutrophils Engage Mitochondrial Metabolism to Circumvent Nutrient Limitations and Maintain Immune Suppression. *Nat Commun* (2018) 9(1):5099. doi: 10.1038/s41467-018-07505-2
52. Anderberg C, Cunha SI, Zhai Z, Cortez E, Pardali E, Johnson JR, et al. Deficiency for Endoglin in Tumor Vasculature Weakens the Endothelial Barrier to Metastatic Dissemination. *J Exp Med* (2013) 210(3):563–79. doi: 10.1084/jem.20120662

**Conflict of Interest:** The authors declare that the research was conducted in the absence of any commercial or financial relationships that could be construed as a potential conflict of interest.

**Publisher's Note:** All claims expressed in this article are solely those of the authors and do not necessarily represent those of their affiliated organizations, or those of the publisher, the editors and the reviewers. Any product that may be evaluated in this article, or claim that may be made by its manufacturer, is not guaranteed or endorsed by the publisher.

Copyright © 2021 Dang, Liu, Hu, Chen, Meng, Hu, Wang, Yuan, Han, Li and Sun. This is an open-access article distributed under the terms of the Creative Commons Attribution License (CC BY). The use, distribution or reproduction in other forums is permitted, provided the original author(s) and the copyright owner(s) are credited and that the original publication in this journal is cited, in accordance with accepted academic practice. No use, distribution or reproduction is permitted which does not comply with these terms.